Solid State Ionics 46 (1991) 299–308
North-Holland

Electrochemical vapor deposition of stabilized zirconia and interconnection materials for solid oxide fuel cells ☆

J. Schoonman, J.P. Dekker, J.W. Broers
Laboratory for Inorganic Chemistry, Delft University of Technology, Julianalaan 136, 2628 BL Delft, The Netherlands

and

N.J. Kiwiet
TNO-Institute of Applied Chemistry, Zeist, The Netherlands

Received 16 January 1991; accepted for publication 5 February 1991

Due to the high operating temperatures (900–1000°C) the material demands upon Solid Oxide Fuel Cell (SOFC) components are quite stringent. Preferably lower operating temperatures (700–800°C) are desired so that gas feed lines, heat exchanges, and structure components can be fabricated from relatively cheap stainless steel components. Typically, the materials used in a SOFC are yttria-stabilized zirconia (YSZ) as the solid electrolyte, nickel-zirconia cermet as the anode, strontium-doped lanthanum manganite as the cathode, and magnesium-doped lanthanum chromite as the interconnection material. The electrolyte and interconnect are difficult to fabricate, because they need to be gas tight, yet thin (30–50 microns) and mechanically stable. Due to the high volatility of CrO_3 the densification of $LaCrO_3$ into thin layers is a more demanding challenge than the fabrication of the electrolyte. Electrochemical Vapor Deposition is the key technology for making thin layers of the solid electrolyte as well as the interconnection material $LaCrO_3$. In the simplest case the oxide growth can be modeled with the Wagner oxidation theory for metals. In this paper theory and experiment of the growth of ionically conducting YSZ and electronically conducting $LaCrO_3$ will be discussed.

1. Introduction

The Solid Oxide Fuel Cell (SOFC) is one of the most studied and valuable applications for oxygen ion conducting solid electrolytes. Solid oxide fuel cells using hydrogen or hydrocarbon fuels and oxygen can generate direct-current electric power. SOFC's have been shown to operate at extremely high fuel efficiency. An advantage fuel cells have over most conventional forms of power generation is that they are not Carnot limited. While many other modes of power generation involve the thermodynamically inefficient intermediate conversion of heat to mechanical energy, fuel cells convert the free energy of a chemical reaction directly to electrical energy. High fuel efficiency and potentially very large power density (W/kg) are therefore possible.

The solid oxide fuel cell holds promise over other types of fuel cells with aqueous, polymeric, or molten electrolytes, because of the high operating temperature and rigid nature of the solid oxide electrolyte.

The high operating temperature of the solid oxide fuel cell ($\sim 1000°C$) has a favorable effect on the reaction kinetics and mass transfer of reactants at the solid electrolyte-electrode-vapor ternary interface. The fast kinetics eliminate the need for expensive noble metal catalysts.

To develop a high energy density solid oxide fuel cell, its weight and the internal resistance of the device must be minimized. The ohmic polarization losses are dependent on the cell design. A variety of configurations are now being considered for the solid

☆ Presented at 2nd Asian Conference on Solid State Ionics (ASSIS-2), October 28–November 1, 1990, Beijing, P.R. China.

oxide fuel cell. These include tubular, monolithic, and planar types.

The following materials are likely to be incorporated into the first generation of solid oxide fuel cell units:

Electrolyte: $Zr_{1-x}Y_xO_{2-x/2}$

Anode: $Ni\text{-}ZrO_2$

Cathode: $La_{1-x}Sr_xMnO_{3-\delta}$

Interconnect: $LaCr_{1-x}Mg_xO_{3-y}$

Fig. 1. summarizes the temperature dependence of the specific resistivities of these SOFC components [1].

The manner in which design can influence the performance is illustrated by examination of the thin-film tubular SOFC configuration adopted by Westinghouse.

In this configuration the thin-film cathode current collection pathway is relatively long, and so this material produces the largest ohmic polarization loss, even though the specific resistivity of the cathode material is substantially lower than that of the solid electrolyte or interconnection material (viz. fig. 1). Table 1 summarizes the ohmic polarization losses [2].

While the solid electrolyte is the highest resistivity material, the data in table 1 reveal the polarization

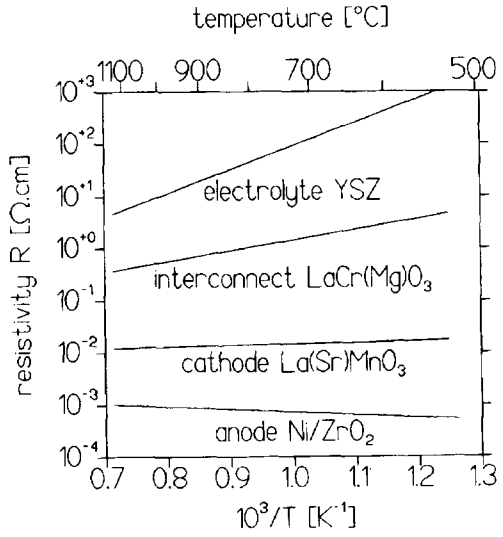

Fig. 1. Specific resistivity-temperature behavior of state-of-the-art SOFC components.

Table 1
Ohmic polarization losses.

Material	R(1000°C) (Ω cm)	Thickness (mm)	Contribution to cell resistance (%)
cathode	0.013	0.07	65
anode	0.001	0.1	25
electrolyte	10.0	0.04	9
interconnect	0.5	0.04	1

loss to be of minor importance in the tubular SOFC configuration. With regard to the numerical values in table 1, it is not surprising to see that many research programs are directed towards the development of novel electrode materials with improved electrical properties. However, the fabrication of thin, gas tight films of the solid electrolyte with improved electrical properties, and electrical interconnection material also attract widespread attention.

Each SOFC design requires a specific processing route. For the solid, electrolyte tapecasting, extrusion and Electrochemical Vapor Deposition (EVD) have been explored for use.

Due to its relative low cost, chemical inertness, and high ionic conductivity, yttria-stabilized zirconia (YSZ) is one of the most widely studied solid electrolytes for the construction of solid oxide fuel cells via the abovementioned processing routes. The interconnection material, i.e. solid solutions based on $LaCrO_3$, cannot be simply sintered to form films at temperatures $< 1200°C$, because the metal ion diffusion rates are extremely low. On the other hand the temperature must be kept as low as possible because of the volatility of the chromium ion. Three processing routes have been suggested, i.e. sintering, RF sputtering and EVD.

In this paper we will review recent experimental and theoretical studies of the EVD process for the fabrication of thin films of the solid electrolyte and interconnection material.

2. Electrochemical vapor deposition

2.1. Solid electrolyte

A technique which has been receiving increasing attention in the past few years is electrochemical va-

por deposition (EVD). EVD is a modified from of chemical vapor deposition (CVD) which utilizes an electrochemical potential gradient to grow thin (1 to 100 microns) non-porous layers of either ionically or electronically conducting metal oxides upon porous substrates. The technique was introduced in 1970 by Isenberg, who was at that time working for Westinghouse [3]. This early work on EVD was not patented, but later, the proven industrial and commercial significance of this technique led to a flood of patents in the 1980's [4]. The primary application of EVD to date has been in fabricating thin layers of the solid electrolyte and interconnection material, used in solid oxide fuel cells.

The steps involved in EVD are shown schematically in fig. 2. The first step in film formation proceeds by a normal CVD type reaction.

Step 1, Pore closure:

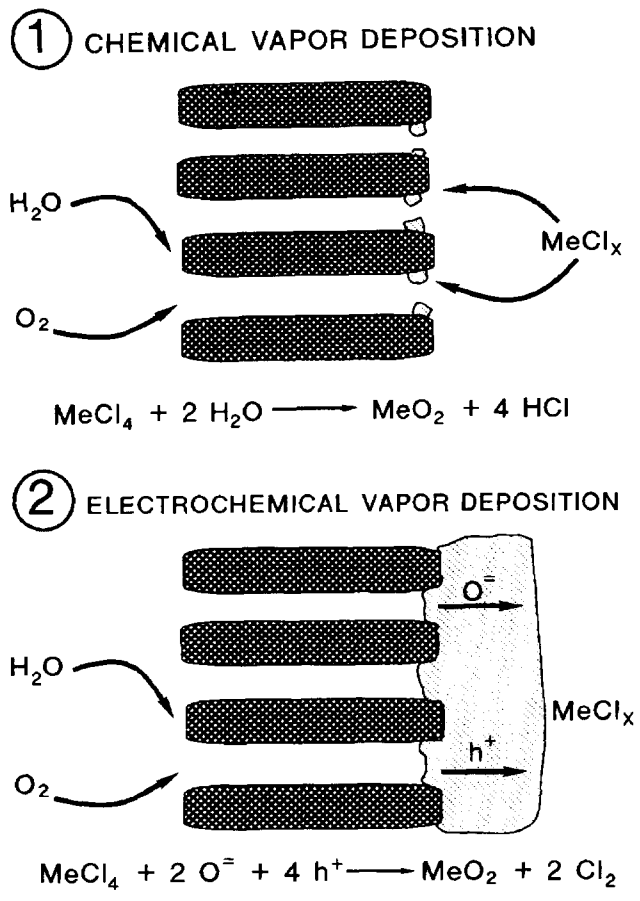

Fig. 2. The CVD and EVD steps in the formation of gas tight metal oxide on a porous substrate

$$MeCl_4 + 2H_2O \rightarrow MeO_2 + 4HCl\,. \quad (1)$$

A porous substrate separates the reactant metal chlorides from a mixture of O_2 and steam. Deposits of the metal oxide form in the pores of the substrate and eventually lead to pore closure.

Once pore closure is complete the reactants are no longer in direct contact. Film growth proceeds due to the large oxygen partial pressure gradient, which exists across the substrate, resulting in the diffusion of oxygen anions from the H_2O/O_2 side to the metal chloride side. The second step, scale growth, proceeds due to the reaction of oxygen anions with metal chlorides.

Step 2, Scale growth:

$$MeCl_4 + 2O^{2-} + 4h^+ \rightarrow MeO_2 + 2Cl_2\,. \quad (2)$$

The first step, pore closure, is very important in determining the ultimate properties of the resulting film. Ideally the CVD phase should form on the metal chloride side, and barely penetrate the porous substrate. The pore plugging layer (the CVD layer) should be thin and as close to the composition of the EVD layer as possible. Carolan and Michaels [5] have modeled the kinetics for pore closure and have shown that the composition of the CVD phase is determined by the molecular diffusivity of the metal chlorides and their relative rates of reaction. In the case of yttria-stabilized zirconia the CVD phase will be depleted of yttria when the reactivity of $ZrCl_4$ is much greater than YCl_3, and enriched when the reactivity of YCl_3 is greater than $ZrCl_4$. Control of the CVD phase is essential to obtaining films with the desired ionic (or electronic) conductivity.

The overall film growth can be rate limited by (a) gas diffusion, (b) surface kinetics on either side of the film or (c) charge transport in the film. When the rate of film growth is governed by solid state diffusion the kinetics are similar to the Wagner oxidation of metals. In Wagner oxidation the rate of scale growth is inversely proportional to the oxide thickness L [6,7]

$$dL/dt = KL^{-1}\,. \quad (3)$$

The integrated form of eq. (3) yields the parabolic rate law

$$L^2 = 2Kt + C_0\,, \quad (4)$$

where C_0 is a constant of integration.

The diffusion processes which take place during EVD growth are shown schematically in fig. 3. Since diffusion through the oxide layer is rate limiting the reactions at the interface are considered to be rapid such that thermodynamic equilibria are established at the oxide/oxygen interface and the metal chloride/oxide interface. The partial pressure of oxygen (P_{O_2}) on the H_2O/O_2 interface is determined by the equilibrium between the gases. Similarly the oxygen partial pressure on the metal chloride side (P''_{O_2}) is determined by the equilibrium between $MeCl_4$, Cl_2, and MeO_2. The large oxygen partial pressure gradient across the film results in a flux of ions and electroneutrality is preserved by an opposing electronic flux. At steady state no net current flows. Thus, the sum over the cationic, anionic, electron and hole currents is zero.

In terms of ionic flux the growth rate can be expressed as [7]:

$$\frac{dL}{dt} = \frac{2}{z} j_i \frac{M}{\rho}, \tag{5}$$

where z is the total electron charge on the cation, ρ is the density, and M the molecular weight of the growing oxide.

In general the ionic flux is given by

$$j_i = -\left\{\frac{kT}{8q^2}\int_{P_{O_2}}^{P''_{O_2}} \sigma_{el}\, d\ln P_{O_2}\right\}\frac{1}{\Delta L}, \tag{6}$$

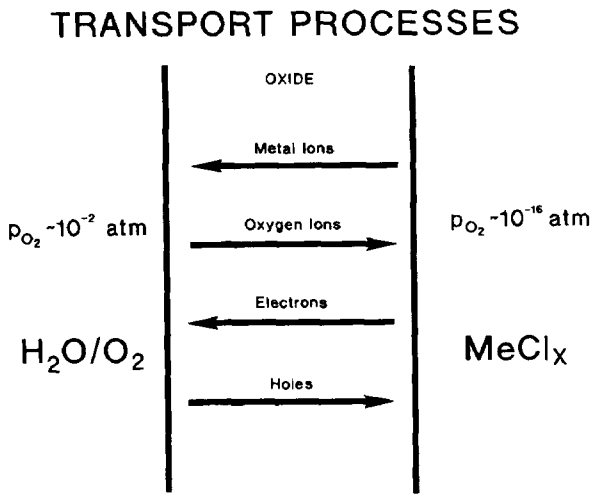

Fig. 3. Diffusion processes during EVD growth of YSZ.

where k is Boltzmann constant, T is absolute temperature, q the charge on an electron and σ_{el} the total electrical conductivity.

From eqs. (5), (6) and the Einstein relation, $\mu_i/D_i = |z_i q|/kT$ the rate constant K for film growth can be derived to yield

$$K = -\frac{1}{16}\frac{M}{\rho N_A} \times\left\{\int_{P_{O_2}}^{P'_{O_2}} [h^{\cdot}] D_{h^{\cdot}} + \int_{P'_{O_2}}^{P''_{O_2}} [e'] D_{e'}\right\} d\ln P_{O_2}, \tag{7}$$

where $[h^{\cdot}]$ and $[e']$ represent the concentration of holes and electrons, $D_{h^{\cdot}}$ and $D_{e'}$ their respective diffusion coefficients, and N_A the Avogadro number. The pressure at which the electronic conductivity changes from n- to p-type is represented by P'_{O_2}. The rate constant can be integrated in two parts to take into account the variation in $[h^{\cdot}]$ and $[e']$ with P_{O_2}.

2.2. Ambipolar diffusion

With regard to the diffusion processes depicted in fig. 3 oxygen ion movement is possible only if at the same time a counterdiffusion occurs of a species with the same charge or if a parallel diffusion occurs of a species with opposite charge. In the stabilized zirconias metal ion diffusion need not be further considered.

Because of their in general higher mobility, the electronic charge carriers diffuse more rapidly than the ionic defects, which causes a local deviation from stoichiometry and hence an electrostatic potential gradient $d\phi/dx$ which will counteract the initial charge separation. From a macroscopic point of view the electroneutrality condition

$$2[V_O^{\cdot\cdot}] + [h^{\cdot}] = [Y'_{Zr}] + [e'] \tag{8}$$

must always be fulfilled, which means that the electrostatic potential gradient forms a link between ionic and electronic charge carriers until the center of the ionic charges and the center of the electronic charges move with the same velocity [14].

The diffusion coefficients which describe the coupled motion of both defect types are called ambi-

polar diffusion coefficients $\tilde{D}$. $\hat{D}$ is dependent on the defect concentrations and self-diffusion coefficients of the charge carriers involved.

The self-diffusion coefficient D_i represents uncorrelated particle diffusion.

For the particle current density j_i the one dimensional Nernst–Planck equation is used. It comprises a diffusion and an electrical field term,

$$j_{V\ddot{o}} = -D_{V\ddot{o}} \frac{d[V_O^{\cdot\cdot}]}{dx} - \frac{2q}{kT} D_{V\ddot{o}} [V_O^{\cdot\cdot}] \frac{d\phi}{dx}, \tag{9}$$

$$j_{e'} = -D_{e'} \frac{d[e']}{dx} + \frac{q}{kT} D_{e'} [e'] \frac{d\phi}{dx}, \tag{10}$$

$$j_{h^{\cdot}} = -D_{h^{\cdot}} \frac{d[h^{\cdot}]}{dx} - \frac{q}{kT} D_{h^{\cdot}} [h^{\cdot}] \frac{d\phi}{dx}. \tag{11}$$

At steady-state the sum over the ionic $j_{V\ddot{o}}$, electron $j_{e'}$, and electron hole $j_{h^{\cdot}}$ fluxes is given by

$$\sum z_i j_i = 0, \tag{12}$$

where z_i is the charge on species i.

For the EVD growth of the stabilized zirconias eq. (12) can be written in the form

$$2j_{V\ddot{o}} + j_{h^{\cdot}} - j_{e'} = 0. \tag{13}$$

Upon substitution of eqs. (8)–(11) into eq. (13) the electrostatic potential gradient $d\phi/dx$ can in principle be derived as a function of the concentrations and self-diffusion coefficients of the migrating defects. Expressing eqs. (9)–(11) in the form

$$j_i = -\tilde{D}_i \frac{dn_i}{dx} \tag{14}$$

and substituting the obtained expression for $d\phi/dx$, then the ambipolar diffusion coefficients can be derived as a function of the defect concentrations and the self-diffusion coefficients of all the charged defects. In order to obtain the derivation, the differentiated forms of eq. (8), and the intrinsic electronic equilibrium constant, $K_{el}(T) = [e'][h^{\cdot}]$ with respect to x are required, i.e.

$$\frac{2d[V_O^{\cdot\cdot}]}{dx} + \frac{d[h^{\cdot}]}{dx} - \frac{d[e']}{dx} = 0, \tag{15}$$

$$\frac{d[e']}{dx} = -\frac{[e']}{[h^{\cdot}]} \frac{d[h^{\cdot}]}{dx}. \tag{16}$$

We shall consider the case of high oxygen partial pressure, $P_{O_2} > 10^{-6}$ atm, and temperatures in the range 1100 to 1300 K. Here YSZ ($x=0.1$) exhibits p-type electronic conductivity, and $[h^{\cdot}] \gg [e']$ holds. Then the reduced electroneutrality condition

$$2[V_O^{\cdot\cdot}] = [Y'_{Zr}] - [h^{\cdot}] \tag{17}$$

holds. Under these conditions we obtain for eq. (9)

$$j_{V\ddot{o}} = -D_{h^{\cdot}} D_{V\ddot{o}} \left[\frac{[h^{\cdot}] + 4[V_O^{\cdot\cdot}]}{D_{h^{\cdot}}[h^{\cdot}] + 4D_{V\ddot{o}}[V_O^{\cdot\cdot}]} \right] \frac{d[V_O^{\cdot\cdot}]}{dx}. \tag{18}$$

With $[h^{\cdot}] \ll [V_O^{\cdot\cdot}] (\sim \frac{1}{2}[Y'_{Zr}])$ and $D_{h^{\cdot}}[h^{\cdot}] \ll D_{V\ddot{o}}[V_O^{\cdot\cdot}]$ eq. (18) reduces to

$$j_{V\ddot{o}} = -D_{h^{\cdot}} \frac{d[V_O^{\cdot\cdot}]}{dx}. \tag{19}$$

In this case, the ambipolar diffusion coefficient $\tilde{D}_{V\ddot{o}}$ equals $D_{h^{\cdot}}$, indicating that the EVD growth is governed by the minority carrier diffusion. Literature data can be used to verify the assumptions made here.

For YSZ($x=0.1$) the temperature dependence of $D_{V\ddot{o}}$ is given by [15]

$$\tilde{D}_{V\ddot{o}} = 1.29 \exp\left(-\frac{1.48\ \text{eV}}{kT} \right) \frac{\text{cm}^2}{\text{s}}. \tag{20}$$

For stabilized zirconias electronic conductivity (σ_{el}) data have been reported in the literature. Together with ionic conductivity (σ_{ion}) data, numerical values for the product $D_{h^{\cdot}}[h^{\cdot}]$ can easily be obtained from the equation for the electronic transference number (t_{el}), i.e.

$$t_{el} = \frac{\sigma_{el}}{\sigma_{ion} + \sigma_{el}}. \tag{21}$$

Upon substituting the Einstein relation into eq. (21) one obtains for the case of hole conductivity

$$[h^{\cdot}] D_{h^{\cdot}} = \frac{kT}{q^2} \frac{t_{h^{\cdot}}}{1 - t_{h^{\cdot}}} \sigma_{ion}. \tag{22}$$

As an example we calculate for the product $[h^{\cdot}] D_{h^{\cdot}}$ values of 8.2×10^{12} to 6.9×10^{13} cm^{-1} s^{-1} at $T = 1273$ K, and $P_{O_2} = 1$ atm for calcia and yttria-stabilized zirconias. From ionic conductivity data we

obtain under these conditions for the product $[V_O^{\cdot\cdot}]\ D_{V_O^{\cdot\cdot}}$ values in the range of 1.4×10^{16} to 9.6×10^{16} cm^{-1} s^{-1} [15–22,25].

For scandia-stabilized zirconia one finds for $[h^{\cdot}]$ $D_{h^{\cdot}} \sim 6.9\times10^{12}$ cm^{-1} s^{-1} and for $[V_O^{\cdot\cdot}]D_{V_O^{\cdot\cdot}}$ values in the range of $(1.4\text{–}1.9)\times10^{17}$ cm^{-1} s^{-1} at $T=1273$ K and $P_{O_2}=1$ atm. It is apparent from these data that the assumptions used to reduce eq. (18) are valid. The EVD growth of stabilized zirconias is governed by the minority carrier diffusion, i.e. eq. (6).

For an ionic conductor the flux is governed by electronic transport, and for an electronic conductor the rate is governed by ionic transport. In growing binary or ternary metal oxides the oxide with the highest minority carrier mobility will be the preferred phase. For example, attempts by Westinghouse to grow yttrium chromite resulted in the formation of chromium oxide doped yttria due to the higher oxygen mobility in chromium oxide doped yttria than in yttrium chromite.

2.3. Interconnection material

The interconnection material $LaCrO_3$ is known to be a *p*-type conductor [23] with a small contribution of oxygen ion conductivity. Because the mobility of the oxygen ions largely exceeds the mobilities of the lanthanum and chromium ions, a contribution of cationic conductivity to the total ionic conductivity can be neglected. For a *p*-type conductor the general expression for the ionic flux is given by

$$j_i = -\left\{\frac{kT}{8q^2}\int_{P'_{O_2}}^{P''_{O_2}} \sigma_{ion}\, d\ln P_{O_2}\right\}\frac{1}{\Delta L}. \tag{23}$$

From eqs. (5), (23), and the Einstein relation the rate constant for film growth is derived to yield

$$K = -\frac{D_{V_O^{\cdot\cdot}}}{6}\int_{P'_{O_2}}^{P''_{O_2}} [V_O^{\cdot\cdot}]\, d\ln P_{O_2}, \tag{24}$$

where $[V_O^{\cdot\cdot}]$ represents the mole fraction of oxygen ion vacancies and $D_{V_O^{\cdot\cdot}}$ its diffusion coefficient. The pressure dependence of $[V_O^{\cdot\cdot}]$ can be understood considering the defect model for magnesium doped $LaCrO_3$. For simplicity it will be assumed that all defects are fully ionized. Mg^{2+} substitutes for Cr^{3+} on a normal lattice side. The acceptor dopant Mg^{2+} can be compensated by a $Cr^{3+}\rightarrow Cr^{4+}$ transition [23] or by the formation of oxygen ion vacancies. This gives the following electroneutrality condition

$$[Mg'_{Cr}] = [h^{\cdot}] + 2[V_O^{\cdot\cdot}],$$

or

$$[Mg'_{Cr}] = [Cr^{\cdot}_{Cr}] + 2[V_O^{\cdot\cdot}]. \tag{25}$$

The defect reaction can be written as

$$O_O^{\times} + 2Cr^{\cdot}_{Cr} \rightarrow 2C_{Cr}^{\times} + V_O^{\cdot\cdot} + \tfrac{1}{2}O_2(g). \tag{26}$$

The equilibrium constant (K_{26}) for reaction (26) is given by

$$K_{26} = \frac{[Cr_{Cr}^{\times}]^2[V_O^{\cdot\cdot}]}{[Cr^{\cdot}_{Cr}]^2[O_O^{\times}]}\, P_{O_2}^{1/2}. \tag{27}$$

In terms of mole fractions the equilibrium constant becomes

$$K_{26} = \frac{(1-2y+2x)^2 x}{(y-2x)^2(3-x)}\, P_{O_2}^{1/2}, \tag{28}$$

where y is the amount of dopant $[Mg'_{Cr}]$ and x is the mole fraction of oxygen deficit $[V_O^{\cdot\cdot}]$. This equation can be solved for x to yield [24]

$$2x = y - \frac{P_{O_2}^{1/2}}{12K_{26}}\left[(24y\,K_{26}P_{O_2}^{-1/2}+1)^{1/2}-1\right]. \tag{29}$$

At low oxygen partial pressures this equation reduces to $2x=y$. In the high P_{O_2} regime the oxygen ion vacancy concentration is much less than the dopant concentration ($x \ll y$). In this case, eq. (29) reduces to:

$$x = 3y^2K_{26}P_{O_2}^{-1/2}. \tag{30}$$

The growth rate constant (eq. (24)) can be integrated in parts. In the low P_{O_2} regime ($2x=y$) the integrated rate constant becomes,

$$K_1 = -\frac{D_{V_O^{\cdot\cdot}}}{12}\, y \ln P_{O_2}\int_{P^B_{O_2}}^{P^A_{O_2}} P^A_{O_2} < P^B_{O_2}. \tag{31}$$

In the middle P_{O_2} regime (eq. (29)) the growth rate constant becomes

$$K_{II} = D_{V\ddot{O}}(F_A(P_{O_2}) - F_B(P_{O_2})) \int_{P^C_{O_2}}^{P^B_{O_2}} \quad P^B_{O_2} < P^C_{O_2}, \tag{32}$$

where $F_A(P_{O_2})$ and $F_B(P_{O_2})$ represent:

$$F_A(P_{O_2}) = \frac{y}{12} \ln P_{O_2}^{-1} \left[\frac{(24yK_{26}P_{O_2}^{-1/2}+1)^{1/2}+1}{(24y\,K_{26}P_{O_2}^{-1/2}+1)^{1/2}-1} \right], \tag{33}$$

$$F_B(P_{O_2}) = \frac{P_{O_2}^{1/2}}{72K_{26}} [1-(24yK_{26}P_{O_2}^{-1/2}+1)^{1/2}]. \tag{34}$$

In the high P_{O_2} regime (eq. (30)) the growth rate constant becomes

$$K_{III} = D_{V\ddot{O}} y^2 K_{26} P_{O_2}^{-1/2} \int_{P^D_{O_2}}^{P^C_{O_2}} \quad P^C_{O_2} < P^D_{O_2}. \tag{35}$$

The overall rate constant is the sum of these three rate constants ($K = K_I + K_{II} + K_{III}$). Numerical data for the equilibrium constant can be obtained from Flandermeyer et al. [31]. However, quantitative values for the growth rate constant cannot be calculated without the knowledge of the oxygen ion diffusion coefficient. To date, no reliable numerical values for $D_{V\ddot{O}}$ are available.

3. EVD results

3.1. Yttria-stabilized zirconia

The variation of the concentrations of the electronic charge carriers, and the diffusion coefficients of these charge carriers have been reported by Weppner [22,25]. This information has been used to numerically calculate the EVD film growth rate of yttria-stabilized zirconia [10]. For 10 mol% (m/o) YSZ the rate of film growth is calculated which results in a film thickness of 6 microns in one hour at 1300 K. The model calculations are in good agreement with the experimental growth rate data of Carolan and Michaels [8]. Kiwiet and Schoonman [26] reported EVD of YSZ on alumina substrates. A layer with thickness of 40 microns grew in four hours, yielding an approximate growth rate constant of 2×10^{-6} cm^2/h. The composition of the YSZ layer corresponded to 10 m/o Y_2O_3.

Experimental results support the application of the Wagner oxidation theory to explain EVD scale growth. Carolan and Michaels [8,9] experimentally found an activation energy of 3.9 eV in the EVD scale growth of 10 m/o yttria-stabilized zirconia, corresponding with reported values of the activation energy of the electron conductivity in YSZ [21,25]. Furthermore, they find that the latter stages of film growth are parabolic in time. Westinghouse [11,12] has also observed parabolic growth rates for the EVD growth of YSZ as well as $LaCrO_3$.

Whether experimentally EVD film growth is rate limited by solid state diffusion depends upon the experimental conditions. The flows of the halide vapors, oxygen and other gases should be maintained above a critical level to eliminate any gas phase control of the EVD reaction. Lin et al. [13] have shown that under certain experimental conditions using substrates with submicrometers pores film growth is limited by the diffusion of gases in the pores of the substrate leading to deposition rates of only 1 to 2 microns per hour.

The characteristic feature of EVD is that film growth is driven by the presence of an electrochemical potential gradient. Under appropriate experimental conditions scale growth is rate limited by the minority carrier diffusion. These characteristics of EVD have both negative and positive aspects. The fact that growth is rate limited by minority carrier diffusion can place limits upon the composition of the metal oxide which can be formed. Furthermore, in order to achieve growth rates on the order of 5 to 10 microns in one hour unacceptable high deposition temperatures may be required. On the other hand a variety of metal oxide thin or thick films can be grown with EVD. Using EVD Westinghouse has grown films of Al_2O_3, Cr_2O_3, doped $LaCrO_3$, and YSZ.

EVD films also display a uniform thickness, due to the fact that the electrochemical potential gradient is the driving force for film growth. Thus where the film is thinnest the driving force is greatest. Through a self-leveling effect very uniform films are formed.

Two types of surface morphology have been observed in EVD growth of YSZ: a faceted type sur-

face, and a cauliflower type surface [8,10]. Extensive studies by Carolan and Michaels varying in reactant concentration and deposition temperature indicated that the morphology was determined by the deposition temperature: with the faceted surface dominating at temperatures below 1300 K, and cauliflower surface dominating at temperatures above 1300 K. The difference in morphology can be explained by a change in relative rates of film growth and surface reconstruction or possibly due to the thermodynamic instability of a surface species at high temperatures [9]. We have modeled the solid state diffusion in YSZ as a function of temperature and dopant concentration [10]. Calculations show that at temperatures below 1300 K both the diffusion of electrons and holes contribute to the overall kinetics for film growth. At temperatures above 1300 K only diffusion of electrons plays a significant role. It is possible that this change in mechanism contributes to the different morphologies observed for the EVD growth of YSZ.

In light of lowering the operating temperature of SOFCs it is of interest to study the growth of better conducting solid electrolytes. Although scandium is by far the best candidate initial work indicates that $ScCl_3$ is too corrosive for practical use in a CVD reactor. Therefore, our current efforts are focused on making EVD films with ytterbium doped zirconia and codoped yttrium, ytterbium films [27].

3.2. Interconnection material

The interconnection material used in SOFCs must have a high electronic conductivity, be stable in both oxidizing and reducing ambients, have a thermal expansion coefficient (TEC) comparable to YSZ, and have no destructive phase transitions within the operation temperature range. Undoped $LaCrO_3$ has a phase transition at 240°C changing from orthorhombic ($TEC = 6.7\times10^{-6}/°C$) to rhombohedral ($TEC = 9.2\times10^{-6}/°C$). Dopants (Mg, Sr, Al) are generally added to change the electrical conductivity, TEC, or phase transition. Both Sr, and Al surpress the orthorhombic/rhombohedral phase transition and adjust the TEC to that of YSZ ($TEC = 10.3\times10^{-6}/°C$). Addition of Mg does little to the TEC or the phase transition. Nonetheless, the current interconnect used in the Westinghouse concept is Mg doped $LaCrO_3$. Early reports on the EVD growth of doped $LaCrO_3$ indicated a problem with the incorporation of dopants into the film [1].

The driving force for scale growth is the formation of the oxide. The difficulty encountered in incorporating other dopants into the $LaCrO_3$ can be that the corresponding chloride is more stable than the oxide. Thus, an excess of the chloride must be added in order to shift the equilibrium to form the oxide [28]. In principle the experiment for growth of $LaCrO_3$ is the same. However controlling the composition and doping is more difficult. The high operating temperatures also pose a problem for in situ growth of these materials on SOFC components.

The modeling of the EVD process of doped $LaCrO_3$ cannot be presented in detail, because numerical values for the oxygen ion diffusion coefficient are lacking. However, a relative growth rate constant K_r can be defined as

$$K_r = K/D_{V\ddot{O}} . \tag{36}$$

For 2 m/o magnesium doped $LaCrO_3$ the logarithm of K_r does not vary linearly with temperature, consequently an overall activation energy of the EVD process cannot be determined.

Pal et al. [11] have observed a growth rate constant of $1.8\times10^{-9}\ cm^2\ s^{-1}$ at 1600 K for 2 m/o magnesium doped $LaCrO_3$. Using this growth rate constant a value of $1\times10^{-7}\ cm^2\ s^{-1}$ is calculated from K_r for $D_{V\ddot{O}}$ (1600 K). From permeability studies on this material [28] at 1273 K $D_{V\ddot{O}}$ is calculated to be $2\times10^{-8}\ cm^2\ s^{-1}$. From these diffusion coefficients the activation energy for oxygen ion diffusion is estimated to be 0.8 eV [24], a value well within the range of activation energies in other perovskite materials [29].

Pal et al. [11] also modeled the kinetics of film growth for $LaCrO_3$–Mg using the defect model of Anderson et al. [30–32]. This model is based on the Schottky equilibrium with equilibrium constant K_s.

$$K_s = [V'''_{La}][V'''_{Cr}][V\ddot{O}]^3 . \tag{37}$$

To determine the oxygen ion vacancy concentration ($[V\ddot{O}]$) as a function of P_{O_2} the following defect reaction was assumed,

$$V'''_{La} + V'''_{Cr} + 6Cr^{\cdot}_{Cr} + 3O^{\times}_{O} \rightarrow \tfrac{3}{2}O_2(g) + 6Cr^{\times}_{Cr} . \tag{38}$$

It is unlikely that this defect reaction determines

the oxygen ion vacancy concentration in $LaCrO_3$–Mg because the presence of cation vacancies, V'''_{La}, V'''_{Cr}, in ternary metal oxides is not favored thermodynamically [33].

There has been very little work to date on the CVD growth of ternary perovskites such as $LaCrO_3$. In our laboratory we are focusing on EVD growth as well as alternative CVD methods to lower the deposition temperature of $LaCrO_3$ thin films.

4. Conclusions

In the modeling of the EVD growth of YSZ it is important to consider the changes in the concentrations of the electronic charge carriers [e′], and [h˙] with P_{O_2}. At high temperatures only electrons need to be considered in EVD growth. At low temperatures the presence of holes at the metal chloride interface may play an important role in the observed faceted morphology of EVD grown YSZ. For the interconnection material $LaCrO_3$ ionic diffusion is rate limiting EVD film growth and very high temperatures (1500 K) are necessary for moderate growth rates. Information on oxygen diffusion in doped $LaCrO_3$ is necessary for a more thorough understanding of the EVD growth.

Perhaps the single most important aspect of EVD grown films is that thin dense gas tight films can be formed. These aspects make EVD industrially a very useful technique in making thin films of otherwise difficult to sinter materials.

References

[1] A.O. Isenberg, Thin Film Bettery/Fuel Cell Power Generating System. Report ERDA, Contract EY-76-C-03-1197 (Westinghouse Electric Corporation, 1978).

[2] B.C.H. Steele, in: Ceramics in Energy Applications: New Opportunities, Proc. Institute of Energy Conf. (Adam Hilger, Bristol, New York, 1990) pp. 173–182.

[3] A.O. Isenberg, Proc. Symp. Electrode Materials and Processes for Energy Conversion and Storage, The Electrochem. Soc. 77-6 (1988);
A.O. Isenberg, Solid State Ionics 3/4 (1981) 431;
W. Feduska and A.O. Isenberg, J. Power Sources 10 (1983) 89.

[4] A.O. Isenberg, U.S. patent no. 4 374 163 (1983);
A.O. Isenberg, U.S. patent no. 4 609 562 (1986);
A. Brian and B.E. Szeders, U.S. patent no. 4 831 965 (1989).

[5] M.F. Carolan and J.N. Michaels, Solid State Ionics 25 (1987) 207.

[6] C. Wagner, Z. Physik. Chem. B21 (1933) 25.

[7] P. Kofstad, Nonstoichiometry, Diffusion and Electrical Conductivity in Binary Metal Oxides (Wiley, New York, 1972).

[8] M.F. Carolan and J.N. Michaels, Solid State Ionics 37 (1990) 189.

[9] M.F. Carolan and J.N. Michaels, Solid State Ionics 37 (1990) 197.

[10] J.P. Dekker, N.J. Kiwiet and J. Schoonman, Solid Oxide Fuel Cells, The Electrochem. Soc. 89-11 (1989) 57.

[11] U.B. Pal and S.C. Singhal, Proc. Sixth (IUPAC) Internat. Conf. High Temperatures–Chemistry of Inorganic Materials, Gaithersburg, MD (1989).

[12] U.B. Pal and S.C. Singhal, Solid Oxide Fuel Cells, The Electrochem. Soc. 89-11 (1989) 41;
U.B. Pal and S.C. Singhal, J. Electrochem. Soc. 137 (1990) 2937.

[13] Y.S. Lin, L.G.J. de Haart, K.J. de Vries and A.J. Burggraaf, Solid Oxide Fuel Cells, The Electrochem. Soc. 89-11 (1989) 67;
Y.S. Lin, L.G.J. de Haart, K.J. de Vries and A.J. Burggraaf, J. Electrochem. Soc. 137 (1990) 3960.

[14] C. Wagner, Z. Physik. Chem. 32 (1936) 447.

[15] S.F. Pal'guev, V.K. Gil'derman and A.D. Neuimin, J. Electrochem. Soc. 122 (1975) 745.

[16] C.H. Perry and A. Feinberg, Solid State Commun. 36 (1980) 519.

[17] T.M. Gur, I.D. Raistrick and R.A. Huggins, Mat. Sci. Eng. 46 (1980) 53.

[18] B. Calès and J.F. Baumard, J. Mat. Sci. 17 (1982) 3243.

[19] H. Näfe, Solid State Ionics 13 (1984) 255.

[20] J.J. Bentzen, N.H. Andersen, F.W. Poulsen, O.T. Sørensen and R. Schram, Solid State Ionics 28–30 (1988) 550.

[21] J.H. Park and R.N. Blumenthal, J. Electrochem. Soc. 136 (1989) 2867.

[22] W. Weppner, J. Solid State Chem. 20 (1977) 305.

[23] W.J. Weber, C.W. Griffin and J.L. Bates, J. Am. Ceram. Soc. 70 (1987) 265.

[24] J.P. Dekker, Electrochemical vapor deposition of solid oxide fuel cell components, M.Sc. Thesis (Delft University of Technology, July 1989).

[25] W. Weppner, Electrochim. Acta 22 (1977) 721.

[26] N.J. Kiwiet and J. Schoonman, IECEC 3 (1990), to be published.

[27] D.J. Vischjager, PhD Thesis (Delft University of Technology, Delft, Netherlands, 1992).

[28] S.C. Singhal, Interconnection material development for solid oxide fuel cells, DOE contract no. DE-AC21-84MC21184, final report (1985).

[29] T. Ishigaki, S. Yamaguchi, K. Koshio, J. Misuzaki and K. Fueki, J. Solid State Chem. 73 (1988) 179.

[30] H.U. Anderson, M.M. Nasrallah, B.K. Flandermeyer and A.K. Agarwal, J. Solid State Chem. 56 (1985) 325.
[31] B.K. Flandermeyer, M.M. Nasrallah, A.K. Agarwal and H.U. Anderson, J. Am. Ceram. Soc. 67 (1984) 195.
[32] B.K. Flandermeyer, M.M. Nasrallah, D.M. Sparlin and H.U. Anderson, High Temp. Sci. 20 (1985) 259.
[33] F.A. Kröger, The Chemistry of Imperfect Crystals. 2, 2nd Rev. Ed. (North-Holland, Amsterdam, 1976).